Flow features of a confined jet impinging onto rough walls

Juliana B. R. Loureiro
Scientific Division, Inmetro, 22.050-050, Rio de Janeiro, Brazil

Rafael C. Alves
Scientific Division, Inmetro, 22.050-050, Rio de Janeiro, Brazil

Atila P. Silva Freire
Mechanical Engineering Program (COPPE/UFRJ), C.P. 68503, 21945-970, Rio de Janeiro, Brazil

Abstract. *The behaviour of a turbulent round jet impinging onto a rough surface is experimentally investigated. The mean and turbulent velocity fields are characterized through laser Doppler anemometry (LDA) and particle image velocimetry (PIV). A near wall parametrization scheme for the mean velocity profile based on stream-wise evolution of the flow characterized by its maximum velocity and the friction velocity is discussed.*

Keywords: *Impinging jet, roughness, law of the wall.*

1. INTRODUCTION

Turbulent jets impinging onto a rough surface are a simple and effective means of promoting the heating or cooling of surfaces. In fact, the number of applications an impinging jet encounters in nature and technology is impressively high. The vertical take-off of aircrafts, the cooling of electronic instruments and the tempering and shaping of glass name only a few of numerous applications.

The natural interest raised by impinging jets has particularly meant that a host of works can be immediately identified in literature on this subject. The contributions to many aspects of the problem are relevant. However, one important issue remains to be adequately tackled: the study of turbulent jets impinging over rough surfaces. The purpose of this work is to fill this gap by producing some quality experimental data on the mean and turbulent fields through laser Doppler anemometry (LDA) and particle image velocimetry (PIV). The work, in particular, proceeds to an analysis the near wall mean-velocity data to investigate the parametrization scheme for the law of the wall proposed by Narasimha et al. (1973) and Özdemir and Whitelaw (1992).

The experimental characterization of an impinging jet onto a rough surfaces is a subject that has long been recognized as deficient. Same contributions have studied the effects that a circular array of protrusions (Beitelmal et al., 2000) or a ring obstacle (Zhou et al., 2009) have on the average heat transfer of an impinging jet. The geometry of these problems is, evidently, very different from extended roughness. Lou et al. (2005) have investigated the effects of geometric parameters on the heat transfer of a confined laminar impinging jet. The study is numerical and resorts to three types of surface: rectangular, sine and triangular wave. Many other works devoted to the numerical investigation of an impinging jet can be found in literature. Typical examples are the direct numerical simulations (DNS) of Hattori and Nagano (2004) and the large eddy simulations (LES) of Hadziabdic and Hanjalic (2008). Both works, however, deal with smooth surfaces. Hadziabdic and Hanjalic (2008), in particular, warn readers that the simulations on smooth surfaces showed "a large sensitivity of results to grid resolution especially in the wall vicinity".

The reference data set presented here for flow over a rough surface is expected to provide an important complement to the smooth wall data of Guerra et al. (2005), helping to establish rigorous conditions to which analytical solutions and numerical simulations of the problem can be tested.

2. THEORY

2.1 Flow of an impinging jet over a smooth surface

The many complex features of an impinging turbulent jet make it a tough case for turbulence modeling. One particular serious difficulty, which is in fact common to all other wall bounded flows, rests on the description of the fine flow length-scales in the near wall region. In the past, the standard procedure to circumvent the problem of specifying a low Reynolds number turbulence closure was to resort to wall functions. The immediate consequence was that just one length-scale equation needed to be specified and flows could be numerically simulated through, for example, a high Reynolds number κ-ϵ model. The great appeal of this scheme was the large computational economy that resulted. Also, and as an extra bonus, wall functions provided a relatively very simple and reliable way to determine the wall shear stress. This fact is very often overlooked by people.

Recently, this very popular practice has been challenged. As computers become more powerful, authors have proposed alternative closure procedures where the turbulence equations are integrated all the way to the wall. These procedures

introduce new variables that are more physically meaningful, with natural boundary conditions at the wall. They may use the concept of eddy-viscosity or second-moment closure. However, irrespective of the type of turbulence model that is chosen, the near wall flow features must be well predicted including the wall shear stress. In addition, complexities introduced by the vortical structures that are formed at the issuing nozzle, by the high streamline curvatures, by the stagnation point and by the entrained flow must also be accounted for.

For wall jets, Patel (1962), Tailland and Mathieu (1967), Ozarapoglu (1973) and Irwin (1973) have reported the existence of a velocity logarithmic region. However, none of these authors could mutually agree on the appropriate functional behavior for the log-law intercept, A. The failure of the conventional law of the wall to be satisfied in wall jets was also verified by Hammond (1982). A further study on the role of the scaling laws in wall jet flows was carried out by Wygnanski et al. (1992).

For an oblique jet, experiments by Özdemir and Whitelaw (1992) have shown that a near wall logarithmic region can be observed well clear of the wall up to the point of maximum velocity. Following a previous recommendation by Narasimha et al. (1973), Özdemir and Whitelaw have introduced a functional behavior for the log-law intercept, A, that uses a scaling procedure based on the stream-wise evolution of the flow characterized by its maximum velocity, U_{max}. The important contribution was the recognition that the nozzle diameter is an inappropriate reference scaling. Thus, local similarity must take into account the flow evolution. To the deviation function, the authors proposed a linear behavior according to expression

$$\frac{u}{u_*} = \frac{1}{\varkappa} \ln\left(\frac{z u_*}{\nu}\right) + A, \tag{1}$$

and

$$A = A_1 \frac{U_{max}}{u_*} - A_2, \tag{2}$$

where $\varkappa$ = 0.4, u_* denotes the friction velocity and A_1 and A_2 are constants.

The velocity logarithmic behavior of an orthogonally impinging jet was further investigated experimentally by Guerra et al. (2005). From an assessment of more than sixty velocity profiles, the authors found that to achieve near wall similarity the reference velocity scale had to be indeed U_{max}.

2.2 Flow over rough surfaces

The effects of roughness on near wall flows can be dramatic. Provided the characteristic size of the roughness elements are large enough, a regime can be established where the flow is turbulent right down to the wall. One important consequence is that the viscous sublayer is completely removed so that a linear solution does not apply anymore. The roughness distorts the logarithmic profile acting as if the entire flow is displaced downwards.

The manner in which the logarithmic law is expressed to describe flow over a rough surface depends on the field of application. In meteorology and industry a common practice is to write

$$\frac{u}{u_*} = \frac{1}{\varkappa} \ln\left(\frac{z}{z_0}\right), \tag{3}$$

where z is the distance above the surface.

The specification of the lower boundary condition on rough walls depends thus on one unknown parameter: the aerodynamic surface roughness, z_0. Many works have attempted to relate the magnitude of z_0 to geometric properties of the surface. Garratt (1992) mentions that the simple relation z_0/h_c = 0.1 (h_c = height of canopy) seems to offer good results for many of the natural vegetation of interest.

In fact, the fundamental concepts and ideas on the problem of a fluid flowing over a rough surface were first established by Nikuradse (1933) who investigated the flow in sand-roughened pipes. Even at that early age, Nikuradse was capable of establishing that, at high Reynolds number, the near wall flow becomes independent of viscosity, being a function of the roughness length, the pipe diameter and Reynolds number. He also found that, for the defect layer, the universal laws apply to the bulk of the flow irrespective of the conditions at the wall. The roughness effects are, therefore, restricted to a thin wall layer.

2.3 Flow of an impinging jet over a rough surface

The previous remarks suggest that a turbulent jet impinging onto a rough surface can be described by

$$\frac{u}{u_*} = \frac{1}{\varkappa} \ln\left(\frac{z}{z_0}\right) + C, \tag{4}$$

and

$$C = C_1 \frac{U_{max}}{u_*} - C_2, \tag{5}$$

where z_0 is a length scale determined by the geometry of the roughness and C_1 and C_2 are constants.

3. EXPERIMENT

A diagram of the experimental apparatus used in the present work is shown in Figure 1a. Air at 20.0 ^{o}C is pumped through a centrifugal blower connected to a 1350 mm long pipe of 43.5 mm internal diameter (D). Inside the pipe a honeycomb section and a series of screens are placed immediately downstream of the contraction in order to make the flow uniform and to control its level of turbulence. Figure 1b presents an illustrative picture of the impinging jet set up. The jet is set to emerge from the circular nozzle with a bulk velocity of 12 m/s. The experiments were conducted for one nozzle-to-plate spacing ($H/D = 2.0$) and Reynolds number of 33,000.

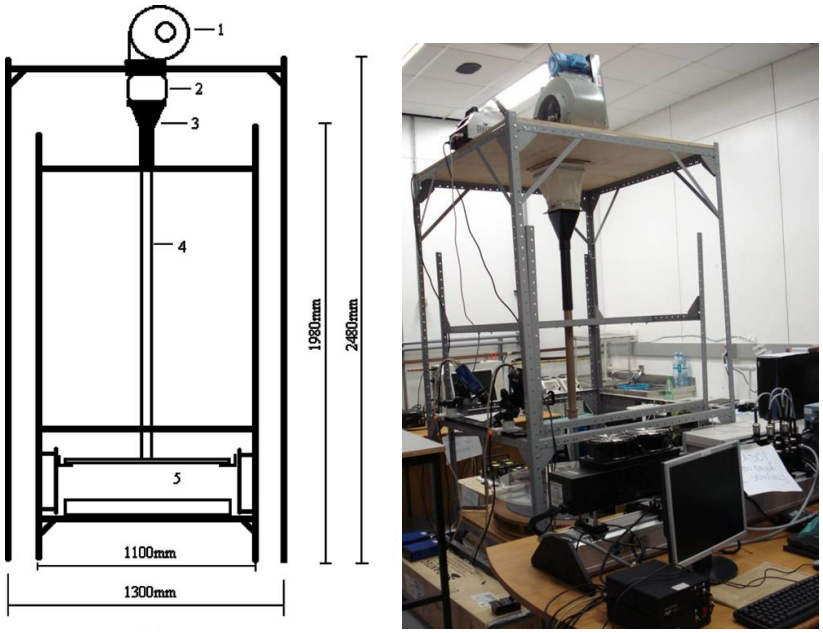

Figure 1. Experimental apparatus: a) overview of the set up: (1) centrifugal blower, (2) flexible section, (3) contraction, (4) pipe, (5) test section; b) illustration of the impinging jet experimental set up.

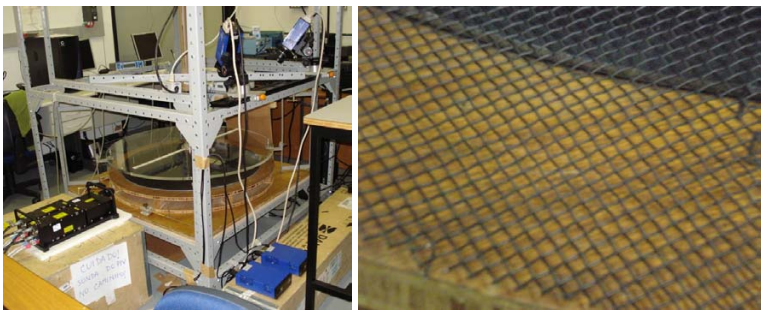

Figure 2. Test section: (a) detail of the impinging and confinement plates; (b) illustration of the rough impingement surface.

The impingement smooth flat surface is made of a 6.0 mm thick aluminum circular sheet. This sheet has 840 mm in diameter and is shown in Figure 2a as a black-painted smooth surface. The controlled parameters in the experiments are the nozzle-to-plate spacing and the stagnation pressure. At each test, the centerline of the jet is lined up with the center of the impingement surface.

To study the influence of the surface roughness on the behaviour of the impinging jet, a stainless steel screen has been placed over the smooth aluminum circular sheet described above. This screen consisted of 0.7 mm diameter wires

distributed in rectangular geometry with open areas of 3.5 x 3.5 mm. An illustration of the rough impingement surface is presented in Figure 2b. Both the rough and smooth surfaces have been painted black in order to minimize reflections from the laser lightsheet and laser beams for the PIV and LDA measurements, respectively.

3.1 Laser Doppler anemometry

The two-component Dantec laser-Doppler anemometry system used a 400 mW Ar-ion tube laser and was operated in the backscatter mode to measure mean and fluctuating velocity fields. A Bragg cell unit was used to introduce a digitally-controlled electronic shift in order to resolve the direction of the flow field and give correct measurements of near-zero mean velocities. The beams were oriented in space such that the green beams measured the wall-parallel velocity component, U, and the blue beams measured the wall-normal component, V. The four light beams that emerged from the 60 mm diameter FiberFlow probe were made to pass through a beam translator and a beam expander with expansion ratio of 1.98. These optical components were used to increase the beam spacing and, as a consequence, to provide a smaller measurement volume with higher laser power thus maximizing the signal to noise ratio. A careful alignment procedure of these optical components were made with the aid of a microscope lens to assure that the four light beams were all crossing precisely at the same point in space where the receiving optical fiber is focused.

Front lens with 800 mm focus length were mounted on the probe to accurately position the measurement volume on the centerline of the impinging jet set up. Before being collected by the photomultipliers, the scattered light was made to pass through interference filters of 514.5 nm and 488 nm, so that only the green and blue lights were received on each photomultiplier, respectively. Table 1 lists the main characteristics of the laser-Doppler system used. The signals from the photomultipliers were digitized and processed through a burst spectrum analyzer BSA P60 operating in single measurement per burst mode. The Dantec BSA Flow Software 4.50 were used to calculate the Doppler frequencies and the resulting velocity samples. A series of LDA biases were avoided by adjusting the strictest parameters on the data processor and software. The level validation and the signal to noise ratio were 8 and 5 respectively. For simultaneous measurements of longitudinal and vertical velocities, a coincidence window of 5,000 μs was used. For the statistics at each point, 50,000 samples were considered.

Table 1. Main characteristics of the laser-Doppler system.

Wavelength	514.5 nm (green) 488nm (blue)
Half-angle between beams	2.791^o
Fringe spacing	5.283 μm (green) 5.011 μm (blue)
Number of fringes	45
Beam spacing	78 mm
Beam diameter	2.2 mm
Dimensions of the measurement volume	
Major axis	4.892 mm (green) 4.640 mm (blue)
Minor axis	238.0 μm (green) 226.0 μm (blue)

Typical uncertainties associated with the mean velocity data – U, W – are below 0.2% of the free stream velocity, u_δ. In regions of reverse flow, the uncertainties increase to about 0.3% of the free stream velocity. Regarding the Reynolds stress components – $\overline{u'u'}$, $\overline{w'w'}$, $\overline{u'w'}$ – uncertainties were estimated to be 2.3%, 1.8% and 4.2% of the square of the friction velocity of the undisturbed flow, respectively. In regions of reverse flow, 3.8%, 3.5% and 6.9% are typical values.

3.2 Particle image velocimetry

The instantaneous velocity field measurements were performed with a LaVision stereoscopic PIV system. The light source was furnished by a double pulsed Nd:YAG laser that produced short duration (10 ns) high energy (120 mJ) pulses of green light (532 nm). The collimated laser beam was transmitted through a set of continuously adjustable cylindrical and spherical lenses to generate a 1 mm thick lightsheet in the region between the jet nozzle and the impinging plate. The light scattered by the seeding particles suspended in the flow was recorded at 15 Hz by the two CCD cameras of 1558 x 1153 pixels and 16-bit resolution. The two cameras were fitted with a Nikkor 50 mm f/1.4D lenses. Image calibration was performed with the use of a 2D calibration target positioned immediately below the nozzle outlet.

For all the measurements the velocity vectors were computed with the aid of LaVision DaVis Software 7.2. Instantaneous velocity fields were obtained by a two-step cross correlation computation, from 64 x 64 pixels to 32 x 32 pixels-size final interrogation regions, with 50% overlap. The pixel resolution is 7.4 x 7.4 μm. Since high quality images were obtained, no particle image preprocessing was necessary. A widely accepted estimation of the absolute displacement error

using self-calibration algorithms is 0.05 pixels. Different thresholds including signal-to-noise ratio and velocity vector magnitude were used as post-processing steps. Residual spurious vectors have been detected using a comparison with the local median of eight neighbour vectors for each grid points. No further filtering has been applied to the velocity fields in order to keep the whole measurement information.

3.3 Seeding

The two measurement techniques used in the present work – the Laser-Doppler anemometry and the Particle image velocimetry – rely on the presence of small seed particles suspended in the flow field. Ideally, the seeding used for laser-based measurements must be small and light enough to follow the fluctuations of the mean flow stream ensuring an adequate aerodynamic response to velocity gradients and turbulence intensities. A compromise between reducing the particle size to improve the flow tracking and increasing the particle volume to improve light scattering and maximizing the signal-to-noise ratio is therefore a very difficult task (Durst et al. 1981). However, since the accuracy of the velocity field determination is ultimately limited by the ability of the scattering particles to follow the instantaneous flow field, a careful choice of the seed particles and a thorough investigation to assure that the seed injection is not affecting the flow field of interest is a time consuming but necessary step of the experimental set up procedure.

In the present work, seeding investigations have used two different types of flow tracers – a fog generator and a Laskin nozzle – and a variety of injection points have been tested. Both flow generators were filled with the same aqueous solution of dialcohol-glycerol mixture. The typical diameter of particles furnished by the fog generator is about 1 μm. The major limitations of fog generators are the intermittent discharge of particles, the high density of the particle flow and the eventual contamination of the surrounding environment by the fog. Droplets produced by the atomizer (Laskin nozzle) vary in size between the range of 0.5 μm to 5.0 μm, with the particle diameter being a function of the pressure of the compressed air feeding line and the working fluid. For the present work, a 5 bar pressure input provided particles of approximately 3 μm in size. Under these conditions, the Laskin nozzle provided a homogeneous and continuous flow of tracer particles, solving the major problems observed with the use of the fog generator.

For both the LDA and PIV techniques the Laskin nozzle provided the best results, assuring a continuously seeded flow with particles that are able to flow field fluctuations but yet scatter enough light to provide a good signal to noise ratio. The investigation for the most appropriate injection position showed that connecting the tracer particles directly to the inlet of the fan furnished the most appropriate homogeneous distribution of the seeds in flow field.

4. RESULTS

The general flow pattern is illustrated through the PIV images shown in Fig. 3. Note the position of the coordinate system. The mean velocity, turbulent kinetic energy and Reynolds shear stress fields are shown.

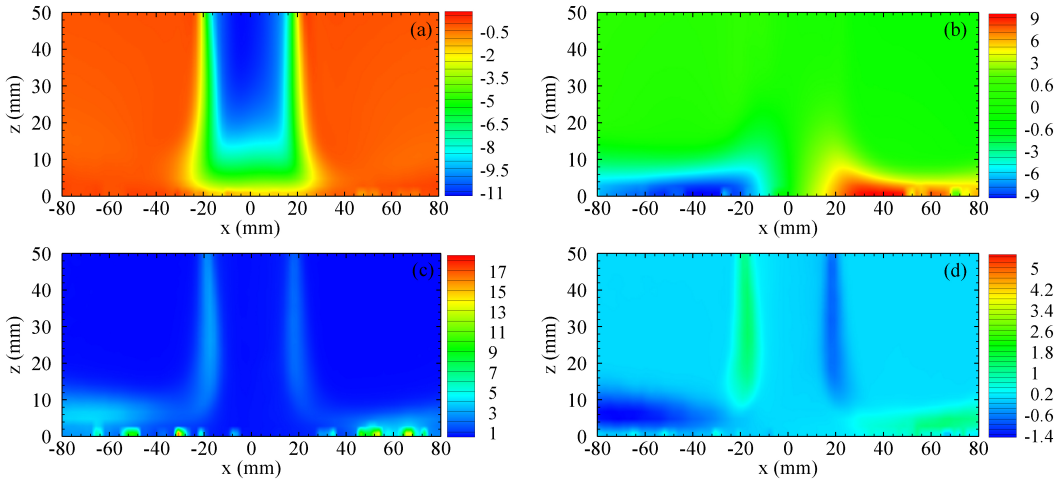

Figure 3. General flow pattern. PIV results: a) axial mean velocity colour map (ms^{-1}), b) radial mean velocity colour map (ms^{-1}), c) turbulent kinetic energy (m^2s^{-2}), d) Reynolds shear stress (m^2s^{-2}).

The work of Phares et al. (2000) splits the flow domain for an unconfined impinging jet into four regions: the free-jet region, the inviscid impingement region, the impinging boundary layer and the wall-jet region. With the PIV results, their identification is easily made.

The axial mean velocity colour map is particularly useful to characterize the free-jet region. The dark blue areas clearly show the downstream vanishing of the jet core due to its interaction with the entrained surrounding fluid and the

effects provoked by the non-penetrability wall condition. The formed stagnation region is illustrated by both the axial and the radial velocity fields.

In the jet deflection region the strong streamline curvatures accelerate the boundary layer until the radial spreading starts to decelerate the flow giving rise to a wall-jet structure. The boundary layer and the wall-jet regions are best characterized by the radial mean velocity colour map. The impinging boundary layer is marked by the dark red region. At about x = -75 mm the wall-jet region begins to develop.

The turbulent mixing layer formed between the potential core and the quiescent fluid is well characterized by the turbulent kinetic energy and Reynolds shear stress figures. Close to the stagnation point the favourable pressure gradients supress turbulence close to the surface. Thus, the main properties of the flow close to the stagnation point are insensitive to the level of turbulence in the free-jet (Kataoka et al., 1982). The high turbulence levels exhibited in the unsteady shear layer that surrounds the free jet are transferred to the boundary layer, inducing turbulence levels that are much higher than those of a canonical boundary layer.

To best characterize the spreading of the wall-jet, the radial components of the mean velocity, turbulence intensity, skewness and flatness distributions were measured at four different radial positions, namely, x = $-$75mm, $-$100mm, $-$125mm and $-$150mm, as presented by Fig. 4.

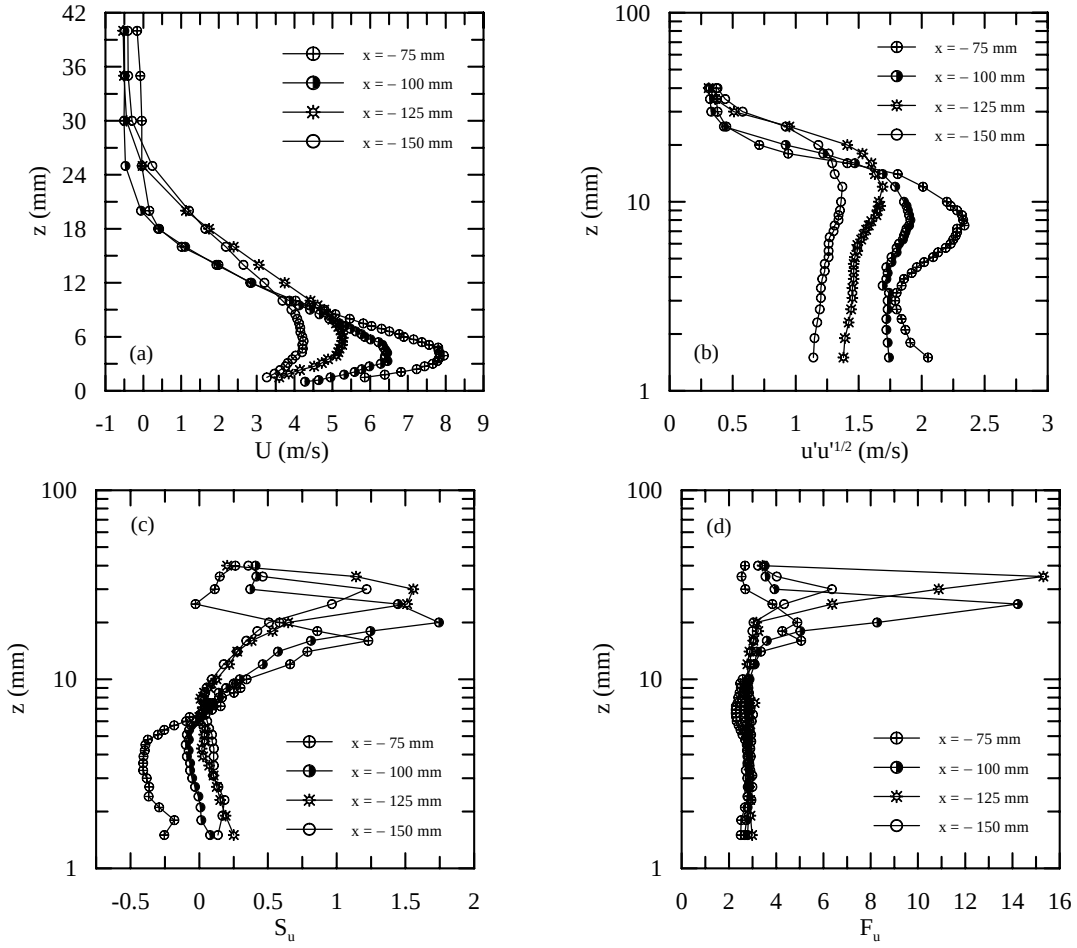

Figure 4. LDA results: a) radial mean velocity profiles, b) radial velocity fluctuations, c) skewness and d) flatness distributions along the impingement plate at stations $x = -75$mm, -100mm, -125mm and -150mm.

In turbulent flows, important structural information can be extracted from the higher-order moments. The skewness and flatness factors for the radial velocity fluctuations are defined by

$$S_u = \overline{u'^3}/\left(\overline{u'^2}\right)^{3/2}, \tag{6}$$

$$F_u = \overline{u'^4}/\left(\overline{u'^2}\right)^{2}. \tag{7}$$

Equivalent expressions can be written for the other flow properties. Data with a Gaussian distribution satisfy S_u = 0 and F_u = 3.

For flow over a smooth wall, S_u is negative throughout the boundary layer. Over rough walls, however, intense positive fluctuations are recorded near to the wall ($S_u \approx 0.5$) and negative in the external region. Flow regions where S_u is positive in a canonical boundary layer are associated with acceleration-dominated velocity fluctuations resulting from the arrival of external high-speed fluid (sweep events). Profiles for the flatness in a boundary layer show very high values near the wall and in the outer layer, where turbulence is highly intermittent.

The value and position of peak velocity for the radial mean velocity distribution is shown in Fig. 4a. The radial turbulent intensity is shown in Fig. 4b, where two peaks can be identified at position x = -75 mm. An increase in x moves the vertical position of the peak location away from the wall and smooths out the near wall behaviour of $\sqrt{uu}$.

Figure 4c shows that position x = -75 mm still suffers the influence of the impinging boundary layer. The negative near wall values of S_u shows that deflected upward flow is still present in the inner boundary layer. At position x = - 150 mm, the flow has nearly relaxed to $S_u \approx 0.5$, approaching the expected trend for a rough wall. Far from the wall, S_u is very large and positive. The flatness distribution presented in Fig. 4d is Gaussian ($F_u \approx 3.0$) provided $z < 10$ mm.

To search for values of u_* and z_0 in Eqs. (4) and (5) global optimization algorithms were used. In general, numerical algorithms for constrained nonlinear optimization can be categorized into gradient based methods and direct search methods. Gradient-based methods use first derivatives (gradients) or second derivatives (Hessians). Direct search methods (Nelder Mead, Differential Evolution, Simulated Annealing, Random Search, etc.) do not use derivative information.

Direct search methods tend to converge more slowly, but can be more tolerant to the presence of noise in the function and constraints. Typically, algorithms only build up a local model of the problems. Also, many such algorithms insist on a certain decrease of the objective function, or decrease of a merit function – which is a combination of the objective and constraints – to ensure convergence of the iterative process. Such algorithms will, if convergent, only find local optima. For this reason they are called local optimization algorithms.

Global optimization algorithms, on the other hand, attempt to find the global optimum by allowing decrease as well as increase of the objective/merit function. Such algorithms are usually computationally more expensive. Here, four different methods were used for solution search: Nelder Mead, Differential Evolution, Simulated Annealing and Random Search. Only when all four methods furnished consistent results, with accuracy down to the sixth decimal fraction, the search was stopped.

The resulting fits for the four positions x = -75mm, -100mm, -125mm and -150mm are shown in Fig. 5.

The relevant flow parameters at the four measuring positions are presented in Table 2. The estimated value of the roughness length for all four positions was $z_0 = 0.2$ mm.

Table 2. Local and global properties of the flow ($z_0 = 0.2$ mm).

Radial stations (mm)	u_* (ms^{-1})	U_{max} (ms^{-1})	C
-75	1.160	7.95	0.01178
-100	0.6864	6.46	2.23035
-125	0.6311	5.28	0.63655
-150	0.3315	4.24	4.82941

The relevant result here is that the functional behaviour of the additive parameter in the law of the wall for impinging jets over smooth surfaces, Eqs. 1 and 2, seems to be valid also for rough surfaces. Figure 6 suggests that

$$C = 0.8432\frac{U_{max}}{u_*} - 5.9615, \tag{8}$$

so that the trends observed by Ozdemir and Whitelaw (1992) and Guerra et al. (2005) regarding the parametrization of the law of the wall in terms of the maximun local velocity and the friction velocity is confirmed.

5. CONCLUSION

The present work has described the behavior of a semi-confined impinging jet over a rough plate. Experimental data for the mean and turbulent fields were obtained by laser Doppler anemometry and particle image velocimetry show that the level of the logarithmic portion of the law of the wall increases with increasing maximum jet velocity. This fact has been observed for the first time for flow over rough surfaces.

The present research is particularly relevant due to its application for the development of methods that can be used for the determination of the local skin-friction for flows over rough surfaces.

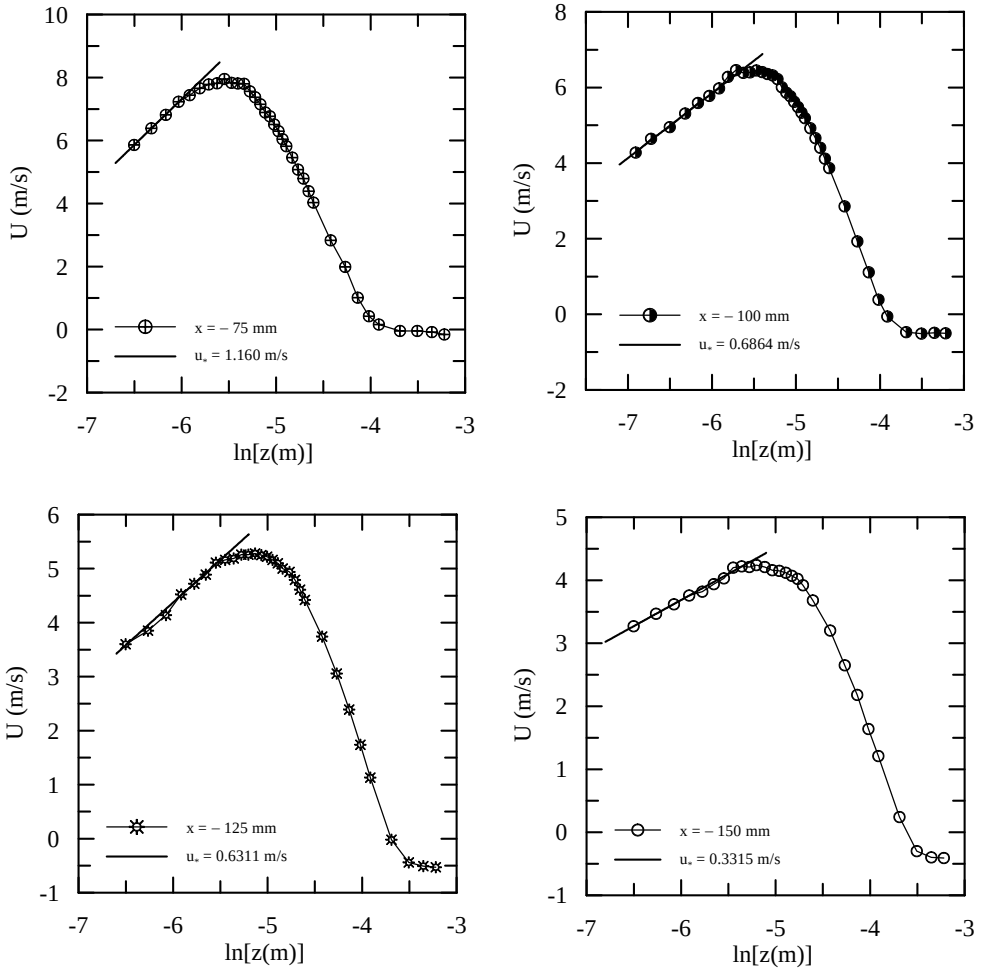

Figure 5. LDA results: Logarithmic velocity profiles along the impingement plate at stations a) $x = -$ 75 mm, b) $x = -$ 100 mm, c) $x = -$ 125 mm and d) $x = -$ 150mm.

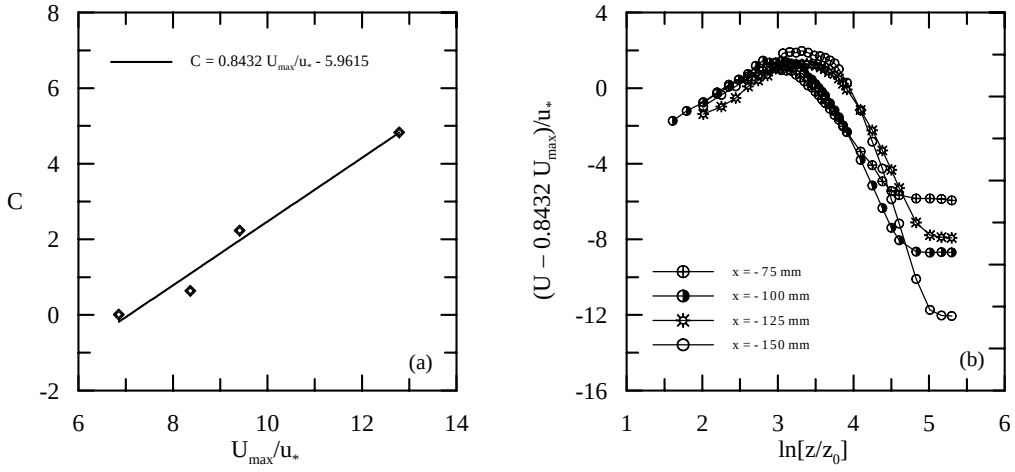

Figure 6. Parametrization of the law of the wall: a) deviation function for the velocity profiles, b) normalized velocity profiles in inner coordinates.

6. ACKNOWLEDGEMENTS

APSF is grateful to the Brazilian National Research Council (CNPq) for the award of a Research Fellowship (Grant No 306977/2006-0). The work was financially supported by the CNPq through Grant No 476091/2007 and by the Rio de Janeiro Research Foundation (FAPERJ) through Grant E-26/170.005/2008.

7. REFERENCES

Baitelmal, A. H. and Saad, M. A., 2000, Effects of surface roughness on the average heat transfer of an impinging air jet, Int. Comm. Heat Mass Transfer, 27, 1-12.

Durst, F., Melling, A. and Whitelaw, J. H., 1981, Principles and practice of laser-Doppler anemometry, London, Academic Press.

Garratt JR (1992) The atmospheric boundary layer. Cambridge University Press, Cambridge

Guerra, D.R.S., Su, J. and Silva Freire, A.P., 2005, The near wall behaviour of an impinging jet, Int. J. Heat and Mass Transfer, 48: 2829-2840.

Guo, Y. and Wood, D. H., 2002, "Measurements in the vicinity of a stagnation point", Exp. Thermal and Fluid Sciences, 25, 605-614.

Hadziabdic, M. and Hanjalic, K., 2008, Vortical structures and heat transfer in a round impinging jet, J. Fluid Mechanics, 596, 221-260

Hammond, G. P., 1982, "Complete velocity profile and "optimum" skin-friction formulas for the plane wall-jet", J. Fluids Engineering, 104, 59-66.

Hattori, H. and Nagano, Y, 2004, Direct numerical calculation of turbulent heat transfer in plane impinging jet, Int. J. Heat Fluid Flow, 25, 749-758.

Irwin, H. P. A. H., 1973, Measurements in a self-preserving plane wall jet in a positive pressure gradient, Journal Fluid Mechanics, 61, 33-63.

Kataoka, K., Kamiyama, Y., Hashimoto, S. and Komai, K., 1982, Mass transfer between a plane surface and an impinging jet, Journal Fluid Mechanics, 119, 91-105.

Lou, Z. Q., Mujumdar, A. S. and Yap, C., 2005, Effects of geometric parameters on confined impinging jet heat transfer, App. Thermal Eng., 25, 2687-2697.

Narasimha, R., Narayan, K. Y. and Pathasarathy, S. P., 1973, Parametric analysis of turbulent wall jets in still air, Aeronaut. J., 77, 335.

Ozarapoglu, V., 1973, Measurements in incompressible turbulent flows, D.Sc Thesis, Laval University, Quebec.

Ozdemir, I. B. and Whitelaw, J. H., 1992, Impingement of an axisymmetric jet on unheated and heated flat plates, J. Fluid Mech., 240, 503-532.

Patel, R. P.,1962, Self preserving two dimensional turbulent jets and wall jets in a moving stream, M.Sc. Thesis, McGill University, Montreal.

Tailland, A. and Mathieu, J., 1967, Jet parietal, J. Mecanique, 6, 1.

Tu, C. V. and Wood, D. H., 1996, Wall pressure and shear stress measurements beneath an impinging jet, Exp. Thermal Fluid Science, 13, 364-373

Zhou, J. W., Wang, Y.G., Middelberg, G. and Herwig, H., 2009, Unsteady jet impingement: heat transfer on smooth and non-smooth surfaces, Int. Comm. Heat and Mass Transfer, 36, 103-110.

Wygnanski, I., Katz, Y. and Horev, 1992, On the applicability of various scaling laws to the turbulent wall jet, J. Fluid Mech., 234, 669-690.